Highly Graphitic Mesoporous Fe,N-Doped Carbon Materials for Oxygen Reduction Electrochemical Catalysts

Donghun Kim,[†] Niels P. Zussblatt,[†] Hoon T. Chung,[‡] Shona M. Becwar,[†] Piotr Zelenay,[‡] and Bradley F. Chmelka*,[†]

[†]Department of Chemical Engineering, University of California, Santa Barbara, California 93106-5080, United States
[‡]Materials Physics and Applications Division, Los Alamos National Laboratory, Los Alamos, New Mexico 87545, United States

S *Supporting Information*

ABSTRACT: The synthesis, characterization, and electro-catalytic properties of mesoporous carbon materials doped with nitrogen atoms and iron are reported and compared for the catalyzed reduction of oxygen gas at fuel cell cathodes. Mixtures of common and inexpensive organic precursors, melamine, and formaldehyde were pyrolyzed in the presence of transition-metal salts (e.g., nitrates) within a mesoporous silica template to yield mesoporous carbon materials with greater extents of graphitization than those of others prepared from small-molecule precursors. In particular, Fe,N-doped carbon materials possessed high surface areas ($\sim$800 m^2/g) and high electrical conductivities ($\sim$19 S/cm), which make

them attractive for electrocatalyst applications. The surface compositions of the mesoporous Fe,N-doped carbon materials were postsynthetically modified by acid washing and followed by high-temperature thermal treatments, which were shown by X-ray photoelectron spectroscopy to favor the formation of graphitic and pyridinic nitrogen moieties. Such surface-modified materials exhibited high electrocatalytic oxygen reduction activities under alkaline conditions, as established by their high onset and half-wave potentials (1.04 and 0.87 V, respectively vs reversible hydrogen electrode) and low Tafel slope (53 mV/decade). These values are superior to many similar transition-metal- and N-doped carbon materials and compare favorably with commercially available precious-metal catalysts, e.g., 20 wt % Pt supported on activated carbon. The analyses indicate that inexpensive mesoporous Fe,N-doped carbon materials are promising alternatives to precious metal-containing catalysts for electrochemical reduction of oxygen in polymer electrolyte fuel cells.

KEYWORDS: *electrocatalyst, nonprecious metal catalyst, graphitic carbon, iron, nitrogen-doped carbon, mesoporous carbon*

1. INTRODUCTION

Polymer electrolyte fuel cells (PEFCs) are promising energy conversion devices that have received significant interest in recent years, due to their high conversion efficiencies, high energy densities, and low environmental impacts.[1,2] However, large-scale applications of PEFCs have been hindered by their high costs, predominantly because of the expensive precious metal platinum- and/or iridium-based catalysts that are used to promote the reduction of oxygen at the cathodes.[3,4] At near-ambient temperatures, the oxygen reduction reaction (ORR) tends to exhibit sluggish kinetics,[3] which have generally been addressed by using undesirably high loadings of Pt-based catalysts on the cathode that exacerbate the cost challenge. In addition, the effectiveness of Pt-based ORR catalysts in direct methanol or ethanol fuel cells (DMFCs or DEFCs) often suffers from fuel crossover and alcohol oxidation at the cathode, which reduces the operating voltage and overall efficiency of the fuel cell.[5,6] Thus, there is significant motivation to develop ORR catalysts that do not rely on

precious metals to achieve comparable or greater activity, selectivity, or stability than existing materials.

By comparison, iron- and nitrogen-doped porous carbon materials exhibit high oxygen reduction activity and selectivity, making these materials promising alternatives to Pt-based precious metal catalysts.[7−12] Judicious selection of precursors[13−17] and optimization of synthesis conditions[18,19] have yielded high ORR activities for carbon-based materials that have been attributed to their high surface areas,[13] high electrical conductivities,[20] or specific nitrogen species (e.g., graphitic nitrogen[21,22] or pyridinic nitrogen[23,24]). In particular, high-surface-area graphitic carbon materials containing Fe and N, such as Fe,N-doped carbon nanotubes,[25] graphene,[26−28] or porous carbon materials,[29] have received significant attention because of their combined high electrical conductivities and good thermal and chemical stabilities.[30−32] High-purity
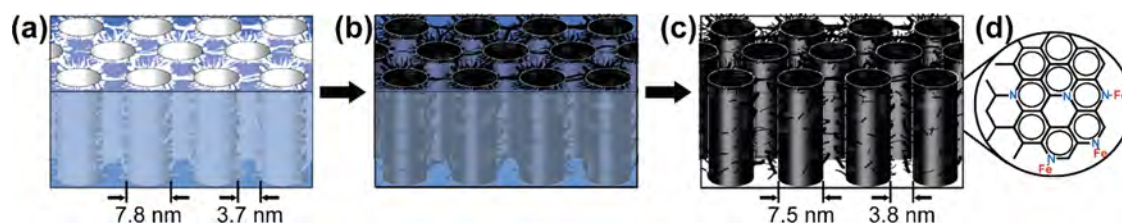
Figure 1. Schematic diagram of the different stages during syntheses of the mesoporous transition-metal and nitrogen-doped carbon materials with highly graphitic properties: (a) initial mesoporous silica template (blue) after calcination, (b) silica−carbon composite after precursor-infiltration and subsequent pyrolysis, and (c) mesoporous carbon (black) after removal of the silica framework. (d) A schematic diagram of different N and Fe,N moieties within graphitic carbon.

nitrogen-doped graphene or carbon nanotubes, grown in the presence of iron, yield electrocatalysts with high ORR activities;[11,33,34] however, their syntheses are relatively complicated. By comparison, mesoporous Fe,N-doped carbons with graphitic properties can be prepared by simple pyrolysis within a sacrificial template, yielding materials with uniform mesopore diameters (2−50 nm) that enable facile diffusion of reactant species to catalytic active sites. In contrast to many conventional carbon materials, such as activated carbon (pore diameters predominantly <2 nm),[35] these larger mesopores facilitate more effective use of available pore surface areas.[36] Previous reports of N- or Fe,N-doped graphitic carbon materials have often relied on the pyrolysis of expensive nitrogen-doped graphitizable precursors, such as macrocyclic porphyrin compounds[22,32] or imidazolium ionic liquids.[31,37] Often, however, volatilization during the pyrolysis process results in low yields of graphitic carbon products.

Here, we report syntheses of transition-metal- and nitrogen-doped mesoporous carbon materials from inexpensive small-molecule organic precursors with improved yields and their characterization to correlate their bulk and surface compositions and structures with their macroscopic electrochemical properties. Using a combination of complementary wide-angle X-ray scattering (WAXS) and Raman spectroscopy analyses, we show that the relative extent of graphitic ordering, which is associated with high electrical conductivity and thermal and chemical stability, depends strongly on the type and quantity of transition-metal species present during pyrolysis. Surface compositions, including nitrogen, oxygen, and transition-metal species, as well as their local bonding environments, are shown to be adjustable to improve the electrocatalytic activities of the product materials, specifically for the technologically important oxygen reduction reaction. Following optimization of bulk and surface compositions, mesoporous Fe,N-containing carbon materials are demonstrated to possess highly graphitic carbon frameworks and exhibit a combination of relatively high surface N contents, high surface areas, high electrical conductivities, and high ORR catalytic activities and selectivities under alkaline conditions that are comparable to commercial platinum electrocatalysts supported on activated carbon.

2. MATERIALS AND METHODS

2.1. Syntheses of Mesoporous Transition-Metal- and N-Doped Carbon Materials. Materials were prepared by pyrolyzing mixtures of an inexpensive high-N-content precursor (melamine), a cross-linking agent (formaldehyde), and transition-metal (Fe, Ni, Co, or Mn) nitrate salts within a mesoporous silica (SBA-15) template, as shown schematically in Figure 1. Mesoporous silica (SBA-15) materials were synthesized by following previously reported protocols.[38] Briefly, 8 g of amphiphilic poly(ethyleneoxide)$_{20}$−

poly(propyleneoxide)$_{70}$−poly(ethyleneoxide)$_{20}$ triblock copolymer (Pluronic P123, Sigma-Aldrich) was dissolved in 60 mL of deionized water and then mixed with 240 mL of 2 M HCl (Fischer Scientific) solution and 17 g of tetraethoxysilane (TEOS, Sigma-Aldrich). After vigorously stirring for 10 min at room temperature to allow the TEOS to hydrolyze, the solution temperature was raised to 40 °C and stirred for an additional 20 h, during which time the hydrolyzed silica precursor species polymerized into a continuous network with mesostructural order directed by the self-assembling P123 triblock copolymer species. Then, stirring was stopped and the solution temperature was raised to 90 °C for 2 days to promote further cross-linking that strengthened the silica framework. After cooling, mesostructured silica powders were recovered by vacuum filtration and calcined in air at 550 °C for 12 h to remove the structure-directing P123 triblock copolymer species, yielding mesoporous silica powder (Figure 1a).

Anhydrous FeCl$_3$ was subsequently grafted onto the pore surfaces of the mesoporous silica to promote the polymerization and graphitization[39] of melamine−formaldehyde resins. Typically, 0.36 g of anhydrous FeCl$_3$ was dissolved in 200 mL of anhydrous ethanol along with 2 g of mesoporous silica powder and stirred for 12 h. After vacuum filtering, the resulting yellow powders were dried at 90 °C for 6 h. For syntheses of mesoporous Ni-, Co-, or Mn-doped carbon materials, equimolar anhydrous AlCl$_3$ was used instead of FeCl$_3$, to eliminate potential contributions of Fe to the ORR electrochemical activity of the non-Fe-containing materials. The roles of AlCl$_3$ and FeCl$_3$ as polymerization and graphitization agents in syntheses of mesoporous Fe,N-doped carbons were compared and shown to exhibit no significant differences in their respective ORR activities, Supporting Information, Figure S1.

Mesoporous transition-metal- and nitrogen-doped carbon materials were synthesized following the general templating method reported by Ryoo et al.,[40] but modified to use a melamine−formaldehyde resin. An alkaline melamine−formaldehyde solution was prepared by mixing 2.05 g of melamine into 3 mL of 0.5 M NaOH, which were subsequently mixed with 2.6 g of aqueous formaldehyde solution (37 wt % formaldehyde, Sigma-Aldrich). Immediately after mixing, this solution was stirred at 75 °C for 30 min and then cooled and neutralized with 1 M HCl aqueous solution, after which transition-metal (Fe, Ni, Co, or Mn) nitrate salts at various transition-metal/melamine molar ratios between 0 and 0.2 were added. Each resulting solution was combined with the FeCl$_3$- or AlCl$_3$-grafted SBA-15 silica and the mixture was sonicated for 30 min within a bath sonicator. After sonication, the excess solution was removed by vacuum filtration and the recovered materials were dried overnight under ambient conditions, followed by heat treatment at 120 °C for 12 h. The materials were further heat-treated at 200 and 350 °C for 6 h at each temperature under N$_2$ atmosphere to increase the degrees of cross-linking of the melamine−formaldehyde resins to reduce volatilization of the carbon and nitrogen precursor species during subsequent pyrolysis. The mesostructured silica−resin materials were then pyrolyzed at 900 °C for 6 h under N$_2$ atmosphere, yielding nonporous mesostructured silica−carbon composites, as shown schematically in Figure 1b. A pyrolysis temperature of 900 °C provides a reasonable trade-off between increased graphitization versus decreased heteroatom content and/or decreased porosity that

tend to occur at higher pyrolysis temperatures, which is consistent with the optimal pyrolysis temperature identified for a melamine-based Fe,N-doped carbon catalyst.[47]

The silica frameworks were subsequently dissolved in 2 M NaOH ethanol/water solution (1:1 volume ratio) with reflux for 12 h (three times). The resulting mesoporous carbon replica materials (Figure 1c) were acid-treated in 0.5 M H$_2$SO$_4$ solution with reflux for 12 h to remove pore-filling carbon residues and excess surface metals, followed by additional pyrolysis at 900 °C for 1 h under N$_2$ to remove surface oxygen species and thereby enhance oxygen reduction electrocatalytic activities. The resulting product materials were composed of graphitic carbon domains, with transition-metal (e.g., Fe) and N moieties present, as shown in the schematic diagram in Figure 1d. For comparison, conventional mesoporous carbon materials were prepared by using an identical method, except with phenol as the precursor instead of melamine.

2.2. Materials Characterization. Thermogravimetric analyses (TGA) of the melamine−formaldehyde materials were conducted by using a METTLER TGA/sDTA851e ThermoGravimetric Analyzer under N$_2$ flow with a ramp rate of 10 °C/min. Residual iron contents of the mesoporous Fe,N-containing carbon materials were estimated from residual mass following high-temperature TGA measurements performed under the flow of dry air. Nitrogen sorption isotherms were acquired at 77 K with MicroMeritics Tristar 3000, and samples were dried overnight at 120 °C under flowing N$_2$ before the measurements. The surface areas were calculated by using the Brunauer−Emmett−Teller (BET) method,[41] whereas pore volumes and size distributions were calculated by using the Barrett−Joyner−Halenda (BJH) method.[42]

X-ray diffraction (XRD) patterns were recorded with a Rigaku Smartlab high-resolution diffractometer with Cu Kα radiation operating at 40 kV and 44 mA. Small-angle XRD patterns were acquired over a 2θ range of 0.5–3.0° with a step size of 0.01°, and wide-angle XRD patterns were acquired over a 2θ range of 10−50° in increments of 0.02°. Raman spectra were obtained by using a home-built Raman spectrometer with blue wavelength excitation at 488 nm. Bulk electrical conductivities were measured by using a Solartron SI 1260 impedance analyzer. X-ray photoelectron spectroscopy (XPS) measurements were conducted on a Kratos Axis Ultra X-ray photoelectron spectroscopy system for approximate surface elemental analyses. Survey XPS scans were performed over the range of 800−100 eV with a pass energy of 160 eV in increments of 0.5 eV, whereas high-resolution XPS scans were conducted for C 1s (296−276 eV) and N 1s (410−390 eV) with a pass energy of 40 eV and a step size of 0.05 eV. Surface elemental compositions were calculated from the areas of the XPS peaks by using Casa XPS 2.3.15 software (CasaSoftware Ltd., Teignmouth, Devon, U.K.) with Gaussian distributions. Relative quantities of surface N species were estimated by deconvolution of the high-resolution XPS spectra into four peaks, corresponding to pyridinic N (398.6 ± 0.3 eV), pyrrolic or pyridonic N (400.5 ± 0.3 eV), graphitic N (401.3 ± 0.3 eV), or nitroxide (402−405 eV) moieties.[43] Images obtained by high-resolution transition electron microscopy were acquired on an FEI Tecnai G2 Sphera microscope operating at 200 kV. Transmission electron microscopy (TEM) samples were prepared by dispersing the materials in ethanol and drop-casting the solution on a carbon-coated copper grid.

2.3. Electrocatalytic Activity Evaluation. Oxygen reduction activities of mesoporous Fe,N-doped carbon catalysts were determined by conducting cyclic voltammetry and linear sweep voltammetry measurements using a CHI Electrochemical Station (Model 750b) in a conventional three-electrode configuration. A rotating-ring disk electrode (RRDE) with a 5.61 mm diameter glassy carbon disk was used as a working electrode, whereas a graphite rod and an Ag/AgCl (3 M NaCl) electrode were used as counter and reference electrodes, respectively. For tests using the rotating-disk electrode (RDE) and rotating-ring disk electrode (RRDE), a Modulated Speed Rotator from Pine Research Instrumentation was used to control the rotation speed of the working electrode. Two milliliters of a catalyst dispersion solution were prepared by mixing catalysts, deionized (Milli-Q) water, and isopropanol (1:3 volume

ratio) with 120 μL of 5 wt % Nafion solution, and 20 μL of the solution were deposited onto the glassy carbon disk of the RRDE electrode to obtain catalyst loadings of 0.60 mg/cm^2 and 0.060 mg$_{Pt}$/cm^2 for mesoporous transition-metal, N-doped carbon catalysts and 20 wt % Pt on activated carbon (Pt/C), respectively. After drying, cyclic voltammograms were recorded at a scan rate of 50 mV/s in 0.1 M NaOH solution saturated with N$_2$ and O$_2$, separately. RRDE tests were conducted using linear sweep voltammetry within an O$_2$-saturated 0.1 M NaOH solution at a scan rate of 5 mV/s. Identical measurements, except those associated with Figures S1 and S4 in the Supporting Information, were also conducted within N$_2$-saturated 0.1 M NaOH solutions and subtracted from the polarization curves acquired in O$_2$-saturated solution to compensate capacitive currents. After the measurements, potentials were converted to the reversible hydrogen electrode (RHE) scale by measuring the potential of a 3 M Ag/AgCl reference electrode vs the RHE. Four-electron selectivities of catalysts were established by using RRDE tests with a platinum-ring electrode potential at a bias potential of 1.2 V. The amount of peroxide formed was estimated from the ring current with a collection efficiency of 37%, according to eq 1

$$H_2O_2\ (\%) = 200 \times \frac{\frac{I_R}{N}}{\frac{I_R}{N} + I_D} \tag{1}$$

where I_R is the ring electrode current, N is the collection efficiency (0.37), and I_D is the disk electrode current.[44] For stability testing, RDE measurements were acquired by linear sweep voltammetry before and after 5000 cyclic voltammetry scans over a range of 0.6−1.0 V vs RHE in an O$_2$-saturated 0.1 M NaOH solution. For the methanol tolerance testing, RDE measurements were performed in O$_2$-saturated solutions of 0.1 M NaOH and 0.5 M MeOH and the half-wave potential acquired from these measurements was compared with the half-wave potential acquired from otherwise identical systems but using solutions without methanol. All electrochemical measurements were conducted at Los Alamos National Laboratory (elevation 2230 m), where the atmospheric pressure is approximately 75% of that at sea level, resulting in correspondingly lower partial pressure of oxygen.

3. RESULTS AND DISCUSSION

Preparation of highly active, high-N-content oxygen reduction catalysts requires that volatilization of the N-containing organic precursors be minimized during the pyrolysis step that is typically needed to generate conductive graphitic materials. This can be achieved by first reacting melamine with formaldehyde to form a melamine−formaldehyde resin in the mesopores of a silica template. Subsequent pyrolysis of the mesostructured melamine−formaldehyde−silica composites in the presence of a metal nitrate salt, such as Fe(NO$_3$)$_3$, yields mesoporous metal, N-doped carbon materials with relatively high nitrogen contents that depend on the cross-linking of the nitrogenous organic precursor species. Use of formaldehyde as a cross-linker improves the yield and N content of the product material. In this work, yield was determined by quantifying the retained mass percentage of the organic components after thermogravimetric analysis (TGA) and near-surface N content was determined by X-ray photoelectron spectroscopy (XPS).

The TGA plot of melamine−formaldehyde resin synthesized with iron nitrate (Figure 2, green) shows that the material exhibits significant mass losses over different temperature regimes, as a result of the different thermal stabilities of the moieties present. Moderate mass loss was observed up to 350 °C (regime I), which is attributed to loss of water from condensation reactions that increase the extent of cross-linking of the melamine−formaldehyde resins and decomposition of iron nitrate salts.[45] Near 350 °C, the material exhibited rapid
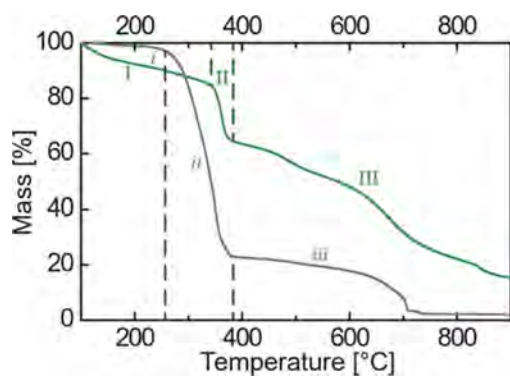
Figure 2. Thermogravimetric analysis plots acquired over the range 100–900 °C under nitrogen atmosphere for melamine–formaldehyde resin and $Fe(NO_3)_3$ mixture (green) and melamine and $Fe(NO_3)_3$, in gray. Distinct regions of mass loss are observed: with formaldehyde present as a cross-linker, regime I corresponds to water loss from polymer condensation or $Fe(NO_3)_3$ decomposition, regime II corresponds to decomposition of methylene cross-links, and regime III corresponds to decomposition of triazine rings. Without formaldehyde, mass loss is due to decomposition of $Fe(NO_3)_3$ (i), amines (ii), and triazine rings (iii). The final product yields after pyrolysis at 900 °C were 15 and 2%, with and without formaldehyde, respectively.

weight loss (regime II), due to the decomposition of methylene cross-links between melamine molecules, and above 400 °C (regime III), a gradual decrease in mass was observed, which has been attributed to decomposition of triazine rings.[46] XPS results (Supporting Information, Table S1) show that the near-surface N/C atom ratio decreased from ~0.93 before pyrolysis to ~0.04 after pyrolysis at 900 °C. This suggests that the significant loss of N from the melamine–formaldehyde resin during pyrolysis is associated with appreciable volatilization of nitrogen species from the carbonaceous networks and is accompanied by restructuring of the carbon networks. Despite the relatively low yield (~85% TGA mass loss after pyrolysis at 900 °C) and low N retention, these values are significantly higher compared to those of materials synthesized without the use of the formaldehyde cross-linker, in which case the volatilization of melamine results in near-complete weight loss (~98%, Figure 2, gray). Without formaldehyde, the mass losses are due to the decomposition of iron nitrate (<250 °C, regime i),[45] amines (250–380 °C, regime ii), and triazine rings (above 400 °C, regime iii).[46] The low retained mass, ~2% after pyrolysis at 900 °C, has previously required that pyrolyzed melamine-based carbon materials be synthesized with high initial loadings of melamine,[34,47] high-surface-area substrates,[16,19,47] or in closed containers during pyrolysis.[14,16,19,34] The inclusion of a cross-linker to reduce melamine volatilization enables mesoporous materials to be synthesized with higher yield and N content (4 atom %) than that previously reported (2.5 atom % N) when melamine alone has been used as a nitrogen source.[16,47] Without cross-linking, syntheses of porous carbons have required substantially higher mass fractions of melamine precursors that are adsorbed and pyrolyzed on high-surface-area carbon substrates[24,47] or the use of closed containers during pyrolysis.[14,16,19] In addition, compared with polymeric nitrogen-containing precursors (e.g., melamine-based resins[29]), the use of small-molecule melamine precursors enables the preparation of porous N–carbon materials by templating.

Because of the possibility for large loss of mass during pyrolysis, mesostructural ordering of carbonaceous materials can be difficult to achieve. After removal of the mesoporous SBA-15 silica template by dissolution at high pH, the mesoporous nitrogen-doped carbon materials exhibit short-range, but not long-range, mesostructural order, as revealed by a combination of scattering and sorption analyses. The small-angle X-ray scattering (SAXS) pattern of mesoporous transition-metal, N-doped carbon material (Supporting Information, Figure S2) shows no distinct reflections and thus no detectable long-range mesostructural order. This is consistent with restructuring of the carbonaceous network as a combined result of the complicated chemistry and longer-range interactions that occur during decomposition of the melamine–formaldehyde resin, volatilization of some pyrolysis products, and silica removal. By comparison, sorption measurements and high-resolution transmission electron microscopy (TEM) images reveal significant short-range mesostructural order. Specifically, N_2 sorption measurements (Supporting Information, Figure S3) revealed type-IV isotherms, indicative of the presence of uniform mesopores,[48] as observed in previously synthesized mesoporous carbons, such as CMK-3.[49] Brunauer–Emmett–Teller (BET)[41] and Barrett–Joyner–Halenda (BJH)[42] sorption analyses were used to determine the specific surface area (800 m²/g), specific pore volume (0.66 cm³/g), and established a narrow pore-size distribution centered about 3.8 nm (Figure 3a). This mean
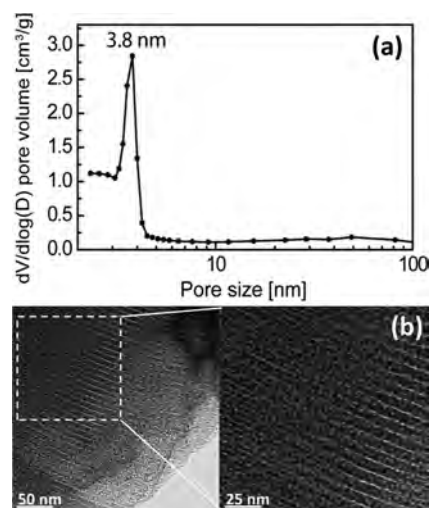

Figure 3. (a) BJH pore-size distribution and (b) representative TEM images of an mesoporous Fe,N-doped carbon material synthesized from melamine–formaldehyde resin with iron nitrate (0.05 iron nitrate-to-melamine mole ratio). The mean pore size of 3.8 nm established in (a) is consistent with the mesopore dimensions (parallel light regions) shown in (b). The wide-angle X-ray diffraction pattern of this material is shown in Figure 5b.

mesopore size corresponds well with the wall thickness of the mesoporous silica templates used to prepare the mesoporous transition-metal, N-doped carbon materials. High surface areas and large pore volumes indicate that mesoporosity is maintained after removal of silica framework. This is corroborated by the high-resolution TEM images of the Fe,N-doped carbon material in Figure 3b, which shows mesopores with dimensions of 3–4 nm between carbonaceous features approximately twice this size. However, the high

extents of mesostructural order appear to be confined to local regions, as they are not evidenced by the SAXS patterns. Nevertheless, the large surface areas, large pore volumes, and uniform mesopore dimensions of the N-doped carbon materials are expected to yield beneficial catalytic properties.

Both short- and long-range graphitic order are present in the melamine−formaldehyde-derived transition-metal- and N-doped mesoporous carbon materials, the extents to which depend strongly on the transition-metal species used. In the presence of transition-metal oxides, the decomposition of the melamine−formaldehyde resin and restructuring of the carbonaceous network at high pyrolysis temperatures (>350 °C) result in materials with increased graphitic properties, compared with materials prepared in the absence of metal species.[50] This is evident in wide-angle X-ray scattering (WAXS) patterns shown in Figure 4a for mesoporous Fe,N-,
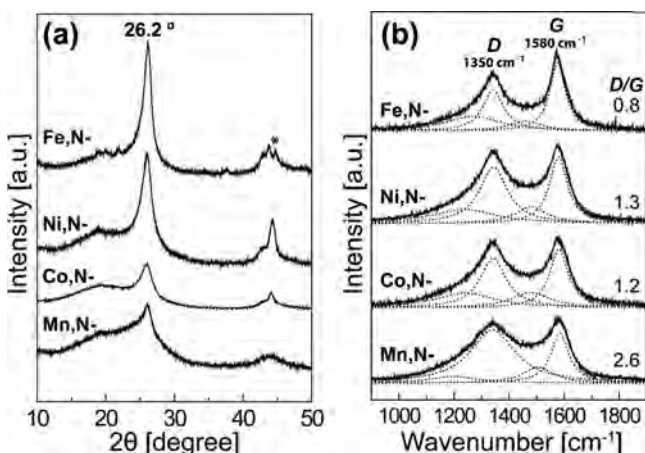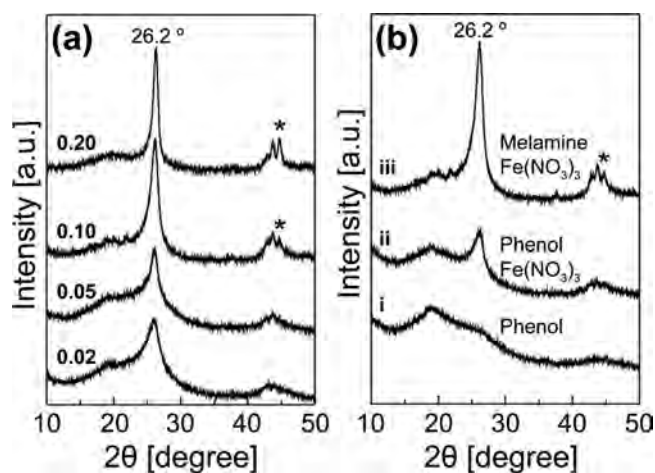

Figure 4. (a) Wide-angle X-ray scattering (WAXS) patterns and (b) Raman spectra of mesoporous Fe,N-, Ni,N-, Co,N-, and Mn,N-doped carbon materials prepared under identical conditions, except for the transition-metal nitrate salt used. The molar ratio of metal nitrate salt to melamine for all materials was 0.10. The WAXS reflections at 26.2° and the Raman bands at 1580 cm^{-1} indicate the highly graphitic properties of the mesoporous Fe,N- and Ni,N-doped carbon materials. A reflection from α-Fe is indicated by the asterisk.

Ni,N-, Co,N-, and Mn,N-doped carbon materials prepared identically, except for the use of the different respective metal nitrate salts. All show reflections at 26.2°, corresponding to a d-spacing of 0.34 nm, which is assigned to the (002) plane of graphitic carbon layers.[51] The mesoporous Fe,N- and Ni,N−carbon materials show sharper (002) reflections, consistent with previous reports that found iron and nickel species to be superior graphitization catalysts for other organic precursors, such as phthalocyanines.[32] By comparison, those formed from Co- or Mn-containing salts exhibit (002) reflections that are significantly less intense. Broad reflections are also observed at lower scattering angles (centered at ca. 20°), which indicate the presence of less-ordered carbon[51] with somewhat larger d-spacing (ca. 0.4 nm). This is consistent with the greater intensities of this reflection relative to the sharper reflection at 26.2° for the less-ordered Mn,N-, Co,N-, and Ni,N-analogues, compared with the Fe,N−carbon materials. All of the mesoporous transition-metal, N-doped carbon materials yield a weaker second reflection at 43.5° that is assigned to the superposition of the (100) and (101) graphitic planes.[51] Additionally, the mesoporous Fe,N−carbon material exhibits a

reflection at 44.5°, likely from metallic α-Fe,[52] which indicates some iron ions were reduced during high-temperature pyrolysis with carbon materials.

WAXS is sensitive to long-range atomic structural order, whereas the positions, relative intensities, and widths of Raman spectroscopy bands are sensitive to locally ordered, as well as disordered, graphitic moieties in mesoporous metal- and nitrogen-doped carbon materials. For example, in the range of 1000−2000 cm^{-1}, Raman spectra of single-crystal graphite exhibit only a narrow band centered at 1575 cm^{-1}, associated with a characteristic lattice-vibration mode of graphite.[53] By comparison, mesoporous Fe,N-, Ni,N-, Co,N-, and Mn,N-doped carbon materials show broad Raman bands (Figure 4b) with two intensity maxima at approximately 1350 and 1580 cm^{-1}. Each of these spectra can be deconvoluted into four Lorentzian-shaped bands centered at 1200, 1350, 1450, and 1580 cm^{-1}. The bands centered at 1350 and 1450 cm^{-1} are associated with relatively disordered graphitic structures that have been attributed to the lattice vibrations of graphite near crystalline domain edges[53] or distorted (e.g., heteroatom-doped) graphitic lattices,[54] respectively. These bands are consistent with the high surface areas of the materials, which are expected to have significant relative fractions of carbon moieties at the edges of crystalline domains or near nitrogen atoms in the graphitic lattices. The broad band centered at 1200 cm^{-1}, by comparison, is attributed to a stretching vibration of polyene-like structures.[55] The dominant peaks centered at 1350 and 1580 cm^{-1} are designated as D and G Raman bands, respectively, and their intensity ratio (D/G) is considered to be inversely correlated with the degree of graphitization.[53,55] Accordingly, the Raman spectra of mesoporous Fe,N-, Ni,N-, Co,N-, and Mn,N-doped carbon materials yield D/G intensity ratios of 0.8, 1.3, 1.2, and 2.6, respectively, which correspond reasonably well with the relative extents of graphitization (Fe > Ni > Co > Mn) observed in the WAXS results. Additionally, the narrowness of the Raman D band has been proposed as another indication of graphitic properties.[56] The full-width-at-half-maximum values were measured to be 92, 124, 115, and 197 cm^{-1} for the mesoporous Fe,N-, Ni,N-, Co,N-, and Mn,N-doped carbon materials, respectively, consistent with their corresponding D/G intensity ratios. Thus, both the Raman and WAXS analyses support the beneficial role of iron nitrate in syntheses of mesoporous Fe,N-doped carbon materials with high extents of graphitization. Furthermore, polarization curves for the mesoporous Fe,N-, Ni,N-, Co,N-, and Mn,N-doped carbon materials (Supporting Information, Figure S4) establish that the Fe,N-doped carbon exhibited greater ORR activity.

Iron is a known graphitizing agent,[32] so the extent of graphitic order depends on the relative quantity of transition-metal used and choice of organic precursor species. Mesoporous Fe,N-doped carbon materials were synthesized with different quantities of iron nitrate (initial iron nitrate/melamine molar ratios of 0.02, 0.05, 0.10, and 0.20), and their graphitic properties were examined by WAXS. As shown in Figure 5a, the relative intensities of the reflections at 26.2° are higher for materials prepared with higher molar ratios of iron nitrate, which indicate higher degrees of graphitic ordering over the range of molar ratios tested. Additionally, these melamine−formaldehyde-derived mesoporous N-doped carbon materials synthesized with transition-metal salts exhibit higher graphitic properties than if other precursors are used. Figure 5b compares the WAXS pattern of a melamine−

Figure 5. Wide-angle X-ray scattering patterns of mesoporous carbon materials prepared under identical conditions by using (a) melamine−formaldehyde resin and $Fe(NO_3)_3$ but with different molar ratios (0.02, 0.05, 0.10, and 0.20) of iron nitrate to melamine and (b) different precursors: (i) phenol−formaldehyde resin without Fe-$(NO_3)_3$, (ii) phenol−formaldehyde resin with $Fe(NO_3)_3$, and (iii) melamine−formaldehyde resin with $Fe(NO_3)_3$. A reflection from α-Fe is indicated by the asterisk.

formaldehyde-derived mesoporous carbon prepared with iron nitrate with that of materials prepared under otherwise identical synthesis conditions, but using phenol−formaldehyde resins[57] without and with the iron nitrate salt. The WAXS pattern of the phenol−formaldehyde-derived mesoporous carbon without iron salt (i) shows only a single broad reflection below 20° and no clear evidence of graphitic ordering. By comparison, when iron nitrate was used, the resulting mesoporous carbon material (ii) exhibited a weak reflection at ∼26° that was much less intense than that for melamine−formaldehyde-derived mesoporous carbon materials (iii). The superior graphitic properties of melamine−resin-derived mesoporous carbons suggest that intermediate species formed during pyrolysis of melamine−formaldehyde resin enable restructuring of the carbonaceous network at high temperature, which results in carbon moieties with greater extents of both local and long-range crystalline order. Although pyrolysis of several similar small-molecule organic precursors with iron or nickel salts has been previously shown to yield materials with graphitic properties,[50] the melamine−form-aldehyde-resin-derived mesoporous carbon materials prepared with iron nitrate appear to exhibit greater extents of graphitization.

The bulk electrical conductivities of these mesoporous transition-metal- and N-doped carbon materials are relatively high and correlate with the degree of graphitization achieved for the different transition-metal nitrates used. Conventional mesoporous carbon materials prepared from phenol−form-aldehyde resin[57] are nongraphitic (as shown in Figure 5b,i) and are therefore expected to have low bulk electrical conductivities due to their high porosities and absence of conductive graphitic domains. Bulk conductivities were determined from impedance measurements for all samples and are tabulated in Supporting Information, Table S2. As expected, the conductivity of the mesoporous carbon material prepared from phenol−formaldehyde was relatively low at 4.6 S/cm. For comparison, graphite powder exhibited a value of 98 S/cm, due to the presence of large crystalline graphitic

domains without significant porosity. In contrast, mesoporous transition-metal- and N-doped carbon materials prepared from melamine−formaldehyde exhibited higher bulk electrical conductivities, in spite of their nitrogen contents that have often been reported to reduce electron conductivities.[58] Although the mesoporous Mn,N-doped carbon with relatively poor graphitic properties exhibited only slightly higher conductivity (7 S/cm) than that of conventional mesoporous carbon materials, the more graphitic mesoporous Fe,N- and Ni,N-doped carbon materials manifested significantly higher bulk electrical conductivities of 19 and 17 S/cm, respectively. Although the mesoporous Fe,N-doped carbon material was less conductive than nonporous graphite (without nitrogen), its conductivity was more than 4 times greater than that of conventional mesoporous carbon materials, which is advantageous for use as an electrocatalyst.

Postsynthesis acid leaching and heat treatment have been demonstrated to increase the oxygen reduction activities of other N-containing carbon materials[20,59,66] and were used similarly here for the mesoporous Fe,N-doped carbon material. Oxygen reduction activities of otherwise identical mesoporous Fe,N-doped carbons, except for their different postsynthesis treatments, were evaluated by rotating ring disk electrode (RRDE) tests in a 0.1 M NaOH electrolyte solution. Polarization curves were measured under alkaline conditions for the (i) as-synthesized mesoporous carbon catalysts, (ii) after acid treatment, and (iii) after acid treatment and additional pyrolysis (900 °C for 1 h under flowing N_2 gas), and the results are shown in Figure 6a and Table 1. As can be seen from the polarization curves in Figure 6a generally shifting to greater absolute current (indicating higher catalytic rates) at higher potentials (indicating smaller required overpotentials), each postsynthesis treatment results in improved electro-catalytic activities. Additionally, peroxide yields (i.e., fraction of O_2 reduced to hydrogen peroxide, rather than water) were calculated from the RRDE ring current by using eq 1 and are plotted as a function of the applied potential in Figure 6b. In addition to resulting in higher electrocatalytic activities, the postsynthesis treatments reduce the generation of peroxides, which improves catalyst efficiency for the four-electron reduction of O_2 to water and thus fuel conversion efficiency.[60] A summary of the electrochemical measurement results, including onset potentials, half-wave potentials, Tafel slopes, and exchange current densities, is provided in Table 1.

As-synthesized mesoporous Fe,N-doped carbon catalysts prepared with alkaline treatment to remove silica templates exhibit a high onset potential of 0.95 V versus RHE, which establishes high ORR activity. However, the reduction current increases slowly as the potential is decreased (Figure 6a,i), resulting in relatively low half-wave potential of 0.76 V and a high Tafel slope of 76 mV/decade (Table 1). As a result, a saturated current−density plateau in the low-potential region (i.e., limiting current density) is not clearly observed. In addition, the Pt ring current reveals that this catalyst produces a significant quantity of peroxide (33% at 0.54 V), indicating significant contributions from the two-electron oxygen reduction process. The two-electron process, which generates peroxides, is less favorable than the four-electron reduction to water, because peroxide lowers the fuel conversion efficiency and can negatively affect the fuel cell membrane and electrode stability.[60] By comparison, following acid treatment to leach out pore-filling carbonaceous materials, the half-wave potential increases to 0.82 V, consistent with a lower Tafel slope of 60
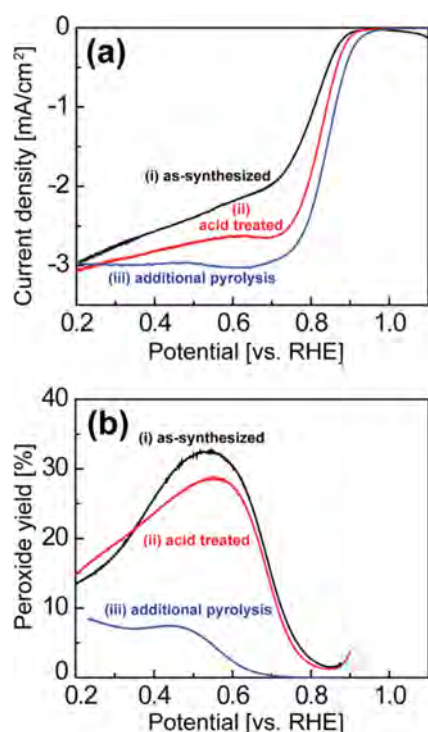
Figure 6. (a) Polarization curves and (b) peroxide yields of mesoporous Fe,N-doped carbon catalysts synthesized using an iron nitrate-to-melamine molar ratio of 0.10, followed by (i) pyrolysis and then alkaline washed to remove the mesoporous silica template (as-synthesized), (ii) after pyrolysis, alkaline washing, and an additional acid treatment, and (iii) after pyrolysis, alkaline washing, acid treatment, and an additional pyrolysis step. These materials were identical to those used in Table 1 and Supporting Information Tables S3 and S4.

mV/decade (Table 1), while the onset potential and peroxide yield are not significantly altered. The decreased value of the Tafel slope after acid treatment indicates that acid leaching removes less-active surface species from the catalysts and/or improves accessibility to active species. However, the catalyst still produces a large quantity of peroxide (maximum peroxide yield of 28% at 0.57 V vs RHE) via the two-electron reduction process. Finally, additional pyrolysis of the acid-treated catalyst significantly improves ORR activities, as established by the higher onset potential (1.02 V), half-wave potential (0.84 V), and four-electron selectivity (maximum peroxide yield reduced to 9% at ∼0.20 V vs RHE), implying that the additional pyrolysis step increased the number of active sites in mesoporous Fe,N-doped carbon catalysts. This is also supported by increased exchange current density and a Tafel slope that is comparable to the catalyst with acid treatment only. On the basis of these results, the acid and heat treatments significantly improve the oxygen reduction activities of the mesoporous Fe,N-doped carbon catalysts.

Increased ORR activities of the mesoporous Fe,N-doped carbon catalysts after postsynthesis treatments can be correlated with increased surface nitrogen and decreased surface oxygen contents. Approximate surface elemental compositions of the mesoporous Fe,N-doped carbon catalysts before and after postsynthesis treatments were estimated and compared by survey X-ray photoelectron spectroscopy (XPS) analyses, and the results are tabulated in Supporting Information, Table S3. Initially, because of the high nitrogen content of melamine-based resin, the melamine−formalde-hyde−silica composite with iron nitrate contained ca. 30 atom % surface N species. By comparison, after the first pyrolysis at 900 °C, the surface nitrogen content decreased significantly to 5 atom %, reflecting the low thermal stability of these nitrogen species at high temperatures. As-synthesized mesoporous Fe,N-doped carbon prepared following alkaline dissolution of the silica frameworks show ca. 4 atom % surface N, 0.7 atom % surface Fe, and 14 atom % surface O contents. The relatively high oxygen content of the material is attributed to surface oxidation during exposure to the alkaline dissolution solution, which offsets the loss of surface oxygen from removal of the silica. Postsynthesis acid treatment of the material leads to lower surface iron content (from 0.7 to 0.1%), consistent with dissolution and removal of Fe species, without other significant changes in surface composition. In conjunction with the electrochemical analyses shown in Figure 6, this suggests that acid treatment exposes surface species that are active for oxygen reduction. Finally, the XPS analysis reveals that the second pyrolysis step at 900 °C, which results in significantly higher ORR activities, further decreases surface oxygen content to ∼3 atom %. Thus, mesoporous Fe,N-doped carbon catalysts prepared under optimized postsynthesis treatment conditions exhibit surface elemental compositions of ∼4 atom % nitrogen and ∼3 atom % oxygen, which are similar to other highly active N-doped carbon-based ORR catalysts.[61]

Complementing the survey XPS estimates of near-surface elemental compositions, high-resolution nitrogen XPS enables the identification of different types of surface nitrogen sites. This specifically includes distinguishing between pyridinic and graphitic nitrogen species that are thought to be associated with ORR active sites.[21,23,62,63] High-resolution N 1s XPS spectra were acquired for mesoporous Fe,N-doped carbon materials after the various synthesis steps shown in Figure 7: (a) with no postsynthesis treatment, (b) after acid treatment, and (c) following acid treatment and additional pyrolysis for 1 h at 900 °C. The quantities of each nitrogen species were estimated by deconvoluting the nitrogen XPS spectra into four peaks: pyridinic and Fe-bonded nitrogen (398.6 eV), pyrrolic and pyridonic nitrogen (400.5 eV), graphitic nitrogen (401.3 eV), and nitrogen oxide (402−405 eV),[43] the results of which are summarized in Supporting Information, Table S4. The low concentrations of surface nitrogen species limit the sensitivity and resolution of the spectra, resulting in overlap of peaks

Table 1. Electrochemical Analyses of the Kinetics of Oxygen Reduction for Mesoporous Fe,N-Doped Carbon Catalysts Synthesized with an Iron Nitrate-to-Melamine Molar Ratio of 0.10 and Different Postsynthesis Treatments

treatments	onset potential (V vs RHE)	half-wave potential (V vs RHE)	Tafel slope[a] (mV/decade)	exchange current density[a] (10^{-5} A/m^2)
as-synthesized	0.95	0.76	76	4.6
acid treatment	0.96	0.82	60	0.46
additional pyrolysis	1.02	0.84	60	1.2

[a]Tafel slopes and exchange current densities were calculated from mass-transport-corrected kinetic current densities.
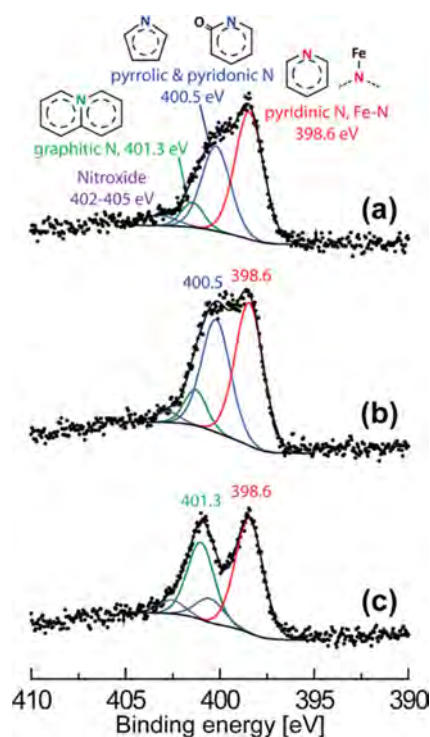
Figure 7. High-resolution X-ray photoelectron spectroscopy (XPS) spectra of mesoporous Fe,N-doped carbon catalysts synthesized with an iron nitrate-to-melamine molar ratio of 0.1 and (a) no postsynthesis treatment, (b) after acid treatment, and (c) after acid treatment and additional pyrolysis for 1 h at 900 °C. These materials are identical to those used in Figure 6, Table 1, and Supporting Information Tables S3 and S4.

associated with pyridinic and Fe-bonded nitrogen, as well as those for the pyrrolic and pyridonic nitrogen moieties, which cannot be distinguished from each other. After alkaline dissolution of the silica template, as-synthesized mesoporous Fe,N-doped carbon catalysts, the materials contain ca. 50 atom % pyridinic or Fe-bonded nitrogen, 35 atom % pyrrolic and/or pyridonic nitrogen, and small amounts of graphitic nitrogen and nitroxide (Figure 7a) as near-surface species. Following acid treatment (Figure 7b), the relative percentages of the pyrrolic and/or pyridonic nitrogen species increased, whereas those of pyridinic or Fe-bonded nitrogen decreased, consistent with acid dissolution of surface iron species. However, after the additional pyrolysis step, the relative percentages of pyrrolic and/or pyridonic nitrogen species significantly decreased and an increase of the percentage of graphitic nitrogen species was observed (Figure 7c). In combination with the electrochemical measurement results, this suggests that pyridinic or graphitic nitrogen species are associated with higher ORR activity than pyrrolic/pyridonic nitrogen species, consistent with several prior findings.[23,63] As the second pyrolysis step reduces the surface oxygen contents significantly, the XPS peak around 400.5 eV can be assigned mainly to pyridonic nitrogen species, which contain oxygen, with a smaller contribution from pyrrolic moieties, which do not. Collectively, the electrochemical measurements and the high-resolution XPS analysis indicate that influencing the distributions of surface nitrogen species presents an opportunity to increase the number of ORR active sites and thus to improve ORR activities.

Besides the types of nitrogen moieties present, the oxygen reduction activities also depend on the amount of Fe species in

mesoporous Fe,N-doped carbon materials, for which there appears to be an optimal value. As discussed previously (Figure 5a), additional iron species are favorable for increasing graphitic properties. However, the amount of iron species that improves ORR activity is generally very low (typically <1.0 atom %),[47,64,65] with excess resulting in iron particles within the graphitic carbon layers. Although surface iron species can be dissolved by acid treatment, encapsulated particles are not readily removed, resulting in potentially considerable amounts of Fe residues[7,52] and a decrease in gravimetric densities of active sites in the catalysts. Mesoporous Fe,N-doped carbon catalysts were prepared with differing iron nitrate-to-melamine molar ratios (0, 0.02, 0.05, 0.10, and 0.20), and their oxygen reduction activities were evaluated by rotating disk electrode tests. As shown in Figure 8a, the mesoporous N-doped carbon
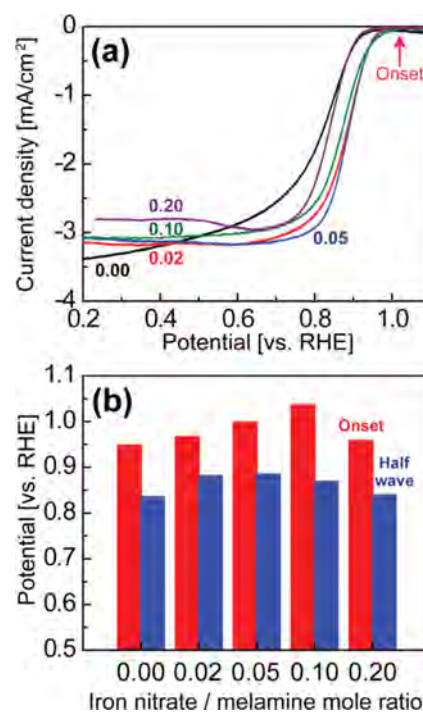
Figure 8. (a) Polarization curves and (b) onset and half-wave potentials of mesoporous Fe,N-doped carbon catalysts prepared under identical conditions including postsynthesis acid treatment and additional pyrolysis, except with different $Fe(NO_3)_3$/melamine molar ratios of 0, 0.02, 0.05, 0.10, and 0.20.

catalyst prepared without iron nitrate exhibited a slowly increasing reduction current with decreasing potential. By comparison, a small quantity of iron nitrate added to the synthesis resulted in a catalyst with higher onset and half-wave potentials. The reduction currents of mesoporous Fe,N-doped carbon catalysts increased at higher molar ratios of iron nitrate-to-melamine, resulting in a maximum onset potential and a maximum half-wave potential observed for the catalysts prepared with 0.05 and 0.10 iron nitrate-to-melamine ratios, respectively. Iron is known to be beneficial for high ORR activity,[66] for which the optimum iron content has been reported to be very low (e.g., 0.05 wt %).[47] Therefore, the greater ORR activities observed here for increasing iron nitrate-to-melamine molar ratios (up to 0.10) suggest that the extent of graphitization is important, as corroborated by the WAXS and Raman results in Figures 4 and 5.

The incorporation of additional iron nitrate, which promotes a higher extent of graphitization, however, eventually led to decreased specific ORR electrocatalytic activity (per mass of catalyst). This is attributed to excess quantities of iron in the carbon frameworks that increase the bulk density of the resulting materials, though do not significantly contribute to increased ORR activity.

On the basis of the TGA results, the catalyst prepared with a 0.20 molar ratio of iron nitrate/melamine is estimated to possess 22 wt % Fe (Supporting Information, Figure S5), resulting in higher bulk densities of the catalysts. A high extent of graphitization, however, tends to be associated with a decreased heteroatom loading or lower porosity, which requires a trade-off between these properties to obtain high ORR activity. Figure 8b separately plots the onset and half-wave potentials measured for the materials prepared with different amounts of iron nitrate. Optimal molar ratios of Fe nitrate/melamine were found to be 0.10 and 0.05 for the highest onset and half-wave potentials, respectively. These results indicate the desirability of optimizing the amount of Fe incorporated into the mesoporous Fe,N-doped carbon materials to obtain high ORR activity.

Highly graphitic mesoporous Fe,N-doped carbon materials prepared under optimized synthesis conditions exhibited high ORR activities under alkaline conditions, that were comparable to commercial carbon-supported 20 wt % Pt/C. Oxygen reduction activities were evaluated by using linear sweep voltammetry in an O_2-saturated 0.1 M NaOH solution with a RDE rotation rate of 900 rpm, as shown in Figure 9a. An optimized mesoporous Fe,N-doped carbon catalyst showed excellent ORR activity with a high onset potential of 1.04 V versus RHE, which is almost identical to that of Pt/C catalysts. Magnified polarization curves of the high-potential region (shown in Supporting Information, Figure S6) more clearly demonstrate the nearly identical onset potentials. This onset potential value is greater than that reported for most transition-metal oxide catalysts (e.g., Ni-doped Co_3O_4 nanowire arrays on graphene foam, for which an onset potential of ∼0.97 V vs RHE has been measured) or N-doped porous carbon materials.[67] It is also close to the values reported for nanostructured N-doped carbon materials, such as carbon nanotube−graphene complexes (1.05 V),[61] carbon nanotube/Fe_3C nanoparticle hybrids (1.07 V),[64] and Fe,N-doped carbon nanofibers on expanded graphite (1.07 V),[65] indicating that the ORR activities of mesoporous Fe,N-doped carbon materials prepared by pyrolysis of inexpensive melamine−formaldehyde can be comparable to high-purity nanostructured carbons. Additionally, the mesoporous Fe,N-doped carbon catalyst showed a half-wave potential of 0.87 V, which is higher than that of the Pt/C catalyst (0.85 V) and is comparable to that of other Fe,N-doped carbon catalysts fabricated from conducting polymer[20] or macrocyclic compounds[66,68] (Table S5). These excellent electrocatalytic activities likely result from a combination of the high mesoporosity and highly graphitic properties of the material, which provide accessible ORR active sites and high electrical conductivity, respectively.

Mesoporous Fe,N-doped carbon also compares favorably to Pt/C catalysts on the basis of Tafel slopes, which were calculated to evaluate their relative electrochemical activities for oxygen reduction. The onset and half-wave potentials are dependent on catalyst loading and the associated density of active sites, as higher catalyst loadings yield increased exchange current densities. However, comparable catalyst loadings
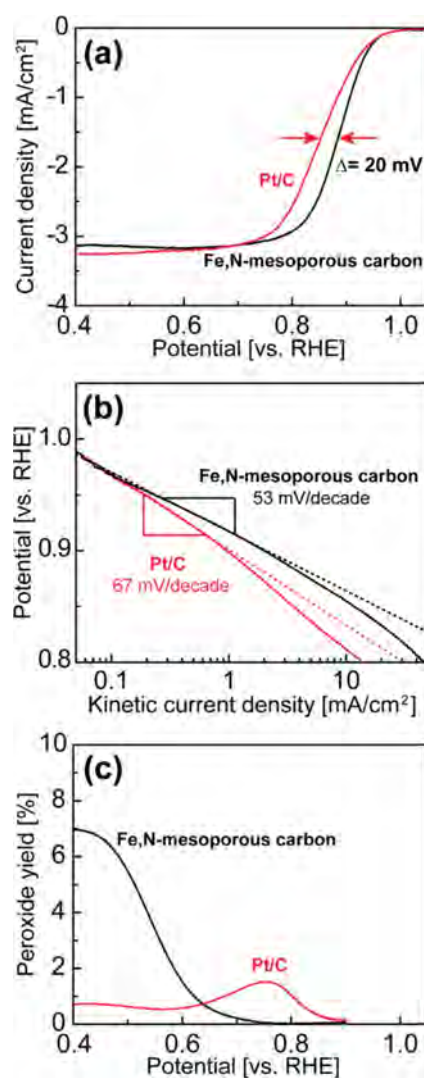
Figure 9. (a) Polarization curves, (b) mass-transport- and iR-loss-corrected Tafel plots, and (c) peroxide yields for Pt/C and for a mesoporous Fe,N-doped carbon catalyst synthesized with an iron nitrate-to-melamine molar ratio of 0.05 and postsynthesis acid and heat treatments. The data were acquired under alkaline conditions (0.1 M NaOH) by linear sweep voltammetry with a rotating ring disk electrode operating at 900 rpm.

cannot be easily determined, as the active sites of Fe,N-doped carbon catalysts are still under debate. Nevertheless, Tafel slopes, which are independent of catalyst loading, can establish relative electrocatalytic activities. Specifically, Tafel slopes of the mesoporous Fe,N-doped catalysts synthesized with an iron nitrate-to-melamine ratio of 0.05 were determined from the slope of iR-loss-corrected overpotential, plotted as a function of logarithmic mass-transport-corrected kinetic current density, and compared with those of commercial Pt/C catalysts. As shown in Figure 9b, the 20 wt % Pt/C catalyst exhibits a Tafel slope of 67 mV/decade, consistent with literature values.[44] By comparison, the mesoporous Fe,N-doped carbon catalyst yields a lower Tafel slope of 53 mV/decade, which is consistent with their higher half-wave potentials, whereas their onset potentials are comparable. The low Tafel slope value, in combination with high onset and half-wave potentials, establishes the fast ORR kinetics of the mesoporous Fe,N-doped carbon catalysts.

The mesoporous Fe,N-doped carbon catalyst was also found to generate less partially reduced peroxide species than the Pt/C catalyst, which contributes to higher energy conversion efficiencies and stabilities of the catalysts. Figure 9c compares the peroxide yields of mesoporous Fe,N-doped carbon and Pt/C catalysts, as determined from RRDE measurements and calculated by using eq 1. The commercially available 20 wt % Pt/C catalyst exhibited a low peroxide yield over the entire potential region, with a maximum of 1.5% at 0.75 V versus RHE. By comparison, the mesoporous Fe,N-doped carbon catalyst generated a negligible amount of peroxide at potentials higher than 0.8 V vs RHE, although the amount of peroxide produced was substantially higher below ~0.6 V; the peroxide yield was ~7% at 0.4 V. This trend is consistent with the small decrease observed in the limiting current of the Fe,N-doped carbon catalyst at potentials below 0.6 V (Figure 9a). The low peroxide yield at high potential is desirable, as Fe,N-doped carbon catalysts often suffer from poor stability of their oxygen reduction activity at high potentials. The peroxide generated from the partial reduction of oxygen has been suggested to oxidize the catalysts or to generate more reactive radicals by coupling with Fe^{2+} ions (e.g., Fenton's reagent), resulting in catalyst degradation.[69] It should be noted that due to the high porosity of the Fe,N-doped carbon, the thickness of its catalyst layer was greater than that for Pt/C so the lower apparent peroxide generation may be due to a combination of higher intrinsic selectivity against peroxide production, greater opportunity for the partially reduced peroxide to be fully reduced to water before exiting the catalyst layer or a higher probability of being decomposed via a non-electrochemical disproportionation reaction. Nevertheless, the low apparent production of peroxide species by the mesoporous Fe,N-doped carbon catalyst at high potentials results in improved electrocatalytic stability, which was evaluated by comparing oxygen reduction activities before and after potential cycling. As shown in Supporting Information, Figure S7, after 5000 cyclic voltammetry scans, the commercially available Pt/C catalysts manifested a 34 mV decrease in the half-wave potential, whereas the mesoporous Fe,N-doped carbon catalysts exhibited a much lower 16 mV decrease in half-wave potential. The smaller decrease in half-wave potential for the mesoporous Fe,N-doped carbon reflects its higher catalytic stability compared to that of Pt/C, which can be attributed to the low apparent peroxide formation, as well as the highly graphitic property of the mesoporous Fe,N-doped carbon catalysts.

Mesoporous Fe,N-doped carbon catalysts also exhibited excellent alcohol tolerance versus platinum-based catalysts. For example, methanol in direct methanol fuel cells (DMFCs) diffuses from the anode to the cathode and is oxidized on Pt-based cathode catalysts, reducing the power output of DMFCs, especially at high voltages.[70] Therefore, high methanol rejection is desirable for ion-conduction membranes, which typically increases the cost of these fuel cells. The effects of methanol were examined for Pt/C and mesoporous Fe,N-doped carbon catalysts by acquiring polarization curves under 0.1 M NaOH without and with 0.5 M methanol, as shown in Supporting Information, Figure S8a,b, respectively. Pt/C catalysts are well known for catalyzing methanol oxidation at the potentials typical of the DMFC cathode operation and show a significant (~360 mV) decrease in their half-wave potentials in the presence of methanol. By comparison, mesoporous Fe,N-doped carbon catalysts exhibit almost

identical polarization curves with and without 0.5 M methanol (~10 mV decrease in half-wave potential), significantly reducing the potentially detrimental effect of methanol fuel crossover. The high oxygen reduction activity, stability, and selectivity of melamine−formaldehyde-derived mesoporous Fe,N-doped carbon catalysts prepared by pyrolysis and additional treatments suggest that they may reduce the cost of PEFCs by both replacing expensive Pt catalysts and also lowering requirements for fuel cell membranes.

4. CONCLUSIONS

Mesoporous N-doped carbon materials with highly graphitic properties have been prepared by pyrolysis of melamine, an inexpensive organic precursor with high N content, form-aldehyde, and iron or nickel nitrate salts. They show high mesoporosities with narrow pore-size distributions (centered at 3.8 nm), which are expected to lead to lower mass transport resistance within the pores and improve accessibility to surface active species. Incorporation of Fe or Ni nitrate salts during synthesis results in higher extents of graphitization compared to other materials prepared by pyrolysis of small molecules. The highly graphitic properties, which include high thermal and chemical stabilities, as well as high electrical conductivity, are favorable for electrode materials. Specifically, mesoporous Fe,N-doped carbon materials show high oxygen reduction electrocatalytic activity under alkaline conditions, and after optimizing surface compositions and Fe loadings, these catalysts exhibit onset and half-wave potentials that are comparable to those of Pt/C catalysts. XPS analyses reveal that the catalysts prepared under optimized synthesis conditions have ~3 atom % surface oxygen and ~4 atom % surface nitrogen species, with most of the nitrogen atoms present in pyridinic or graphitic nitrogen moieties, which appear to be associated with ORR active sites. Correlation of ORR activity with the relative populations of these nitrogenous moieties provides insights into catalytically active sites of N-doped carbon materials. The electrocatalysts also show superior stability, as well as higher selectivity to oxygen reduction in the presence of methanol. The favorable oxygen reduction properties of mesoporous Fe,N-doped carbon catalysts, synthesized from inexpensive commodity small-molecule precursors, are expected to make them attractive in diverse electrochemical applications.

■ ASSOCIATED CONTENT

ⓢ Supporting Information
The Supporting Information is available free of charge on the ACS Publications website at DOI: 10.1021/acsami.8b06009.

> Composition information for cross-linked and pyrolyzed melamine−formaldehyde; bulk electrical conductivities of carbon materials prepared with various precursors; surface elemental compositions and relative percentages of nitrogen-containing moieties; values of electro-chemical activity parameters; polarization curves of mesoporous Fe,N-doped carbon materials prepared by grafting mesoporous silica with $FeCl_3$ vs $AlCl_3$; small-angle X-ray scattering pattern and nitrogen sorption curves of mesoporous Fe,N-doped carbon; polarization curves acquired for Mn,N-, Ni,N-, Co,N-, Pt/C, and mesoporous Fe,N-doped carbon catalysts; thermogravi-metric analysis curve used to determine embedded iron composition; durability testing of Pt/C and mesoporous

Fe,N-doped carbon catalysts; and selectivity comparisons of the catalysts based on polarization curves acquired without and with the presence of methanol (PDF)

■ AUTHOR INFORMATION

Corresponding Author
*E-mail: bradc@engineering.ucsb.edu.

ORCID
Donghun Kim: 0000-0003-4080-5869
Niels P. Zussblatt: 0000-0002-1717-0722
Bradley F. Chmelka: 0000-0002-4450-6949

Notes
The authors declare no competing financial interest.

■ REFERENCES

(1) Jacobson, M. Z.; Colella, W. G.; Golden, D. M. Cleaning the Air and Improving Health with Hydrogen Fuel-Cell Vehicles. *Science* **2005**, *308*, 1901−1905.

(2) Schultz, M. G.; Diehl, T.; Brasseur, G. P.; Zittel, W. Air Pollution and Climate-Forcing Impacts of a Global Hydrogen Economy. *Science* **2003**, *302*, 624−627.

(3) Gewirth, A. A.; Thorum, M. S. Electroreduction of Dioxygen for Fuel-Cell Applications: Materials and Challenges. *Inorg. Chem.* **2010**, *49*, 3557−3566.

(4) Strickler, A. L.; Jackson, A.; Jaramillo, T. F. Active and Stable Ir@Pt Core-Shell Catalysts for Electrochemical Oxygen Reduction. *ACS Energy Lett.* **2017**, *2*, 244−249.

(5) Wang, J.-T.; Wasmus, S.; Savinell, R. F. Real-Time Mass Spectrometric Study of the Methanol Crossover in a Direct Methanol Fuel Cell. *J. Electrochem. Soc.* **1996**, *143*, 1233−1239.

(6) Gurau, B.; Smotkin, E. S. Methanol Crossover in Direct Methanol Fuel Cells: A Link between Power and Energy Density. *J. Power Sources* **2002**, *112*, 339−352.

(7) Wu, G.; More, K. L.; Johnston, C. M.; Zelenay, P. High-Performance Electrocatalysts for Oxygen Reduction Derived from Polyaniline, Iron, and Cobalt. *Science* **2011**, *332*, 443−447.

(8) Li, Q.; Cao, R.; Cho, J.; Wu, G. Nanocarbon Electrocatalysts for Oxygen Reduction in Alkaline Media for Advanced Energy Conversion and Storage. *Adv. Energy Mater.* **2014**, *4*, No. 1301415.

(9) Tylus, U.; Jia, Q.; Strickland, K.; Ramaswamy, N.; Serov, A.; Atanassov, P.; Mukerjee, S. Elucidating Oxygen Reduction Active Sites in Pyrolyzed Metal-Nitrogen Coordinated Non-Precious-Metal Electrocatalyst Systems. *J. Phys. Chem. C* **2014**, *118*, 8999−9008.

(10) Zhang, M.; Dai, L. Carbon Nanomaterials as Metal-Free Catalysts in Next Generation Fuel Cells. *Nano Energy* **2012**, *1*, 514−517.

(11) Gong, K.; Du, F.; Xia, Z.; Durstock, M.; Dai, L. Nitrogen-Doped Carbon Nanotube Arrays with High Electrocatalytic Activity for Oxygen Reduction. *Science* **2009**, *323*, 760−764.

(12) Sebastián, D.; Serov, A.; Matanovic, I.; Artyushkova, K.; Atanassov, P.; Aricò, A. S.; Baglio, V. Insights on the Extraordinary Tolerance to Alcohols of Fe-N-C Cathode Catalysts in Highly Performing Direct Alcohol Fuel Cells. *Nano Energy* **2017**, *34*, 195−204.

(13) Yang, W.; Fellinger, T.-P.; Antonietti, M. Efficient Metal-Free Oxygen Reduction in Alkaline Medium on High-Surface-Area Mesoporous Nitrogen-Doped Carbons Made from Ionic Liquids and Nucleobases. *J. Am. Chem. Soc.* **2011**, *133*, 206−209.

(14) Nallathambi, V.; Leonard, N.; Kothandaraman, R.; Barton, S. C. Nitrogen Precursor Effects in Iron-Nitrogen-Carbon Oxygen Reduction Catalysts. *Electrochem. Solid-State Lett.* **2011**, *14*, B55−B58.

(15) Wu, G.; Zelenay, P. Nanostructured Nonprecious Metal Catalysts for Oxygen Reduction Reaction. *Acc. Chem. Res.* **2013**, *46*, 1878−1889.

(16) Ganesan, S.; Leonard, N.; Barton, S. C. Impact of Transition Metal on Nitrogen Retention and Activity of Iron-Nitrogen-Carbon Oxygen Reduction Catalysts. *Phys. Chem. Chem. Phys.* **2014**, *16*, 4576−4585.

(17) Dombrovskis, J. K.; Palmqvist, A. E. C. One-Pot Synthesis of Transition Metal Ion-Chelating Ordered Mesoporous Carbon/Carbon Nanotube Composites for Active and Durable Fuel Cell Catalysts. *J. Power Sources* **2017**, *357*, 87−96.

(18) Dorjgotov, A.; Ok, J.; Jeon, Y.; Yoon, S. H.; Shul, Y. G. Activity and Active Sites of Nitrogen-Doped Carbon Nanotubes for Oxygen Reduction Reaction. *J. Appl. Electrochem.* **2013**, *43*, 387−397.

(19) Gumeci, C.; Leonard, N.; Liu, Y.; McKinney, S.; Halevi, B.; Barton, S. C. Effect of Pyrolysis Pressure on Activity of Fe-N-C Catalysts for Oxygen Reduction. *J. Mater. Chem. A* **2015**, *3*, 21494−21500.

(20) Tran, T.-N.; Song, M. Y.; Singh, K. P.; Yang, D.-S.; Yu, J.-S. Iron-polypyrrole Electrocatalyst with Remarkable Activity and Stability for ORR in Both Alkaline and Acidic Conditions: A Comprehensive Assessment of Catalyst Preparation Sequence. *J. Mater. Chem. A* **2016**, *4*, 8645−8657.

(21) Lai, L.; Potts, J. R.; Zhan, D.; Wang, L.; Poh, C. K.; Tang, C.; Gong, H.; Shen, Z.; Lin, J.; Ruoff, R. S. Exploration of the Active Center Structure of Nitrogen-Doped Graphene-Based Catalysts for Oxygen Reduction Reaction. *Energy Environ. Sci.* **2012**, *5*, 7936−7942.

(22) Liu, R.; Wu, D.; Feng, X.; Müllen, K. Nitrogen-Doped Ordered Mesoporous Graphitic Arrays with High Electrocatalytic Activity for Oxygen Reduction. *Angew. Chem., Int. Ed.* **2010**, *49*, 2565−2569.

(23) Kundu, S.; Nagaiah, T. C.; Xia, W.; Wang, Y.; Van Dommele, S.; Bitter, J. H.; Santa, M.; Grundmeier, G.; Bron, M.; Schuhmann, W.; Muhler, M. Electrocatalytic Activity and Stability of Nitrogen-Containing Carbon Nanotubes in the Oxygen Reduction Reaction. *J. Phys. Chem. C* **2009**, *113*, 14302−14310.

(24) Wu, J.; Ma, L.; Yadav, R. M.; Yang, Y.; Zhang, X.; Vajtai, R.; Lou, J.; Ajayan, P. M. Nitrogen-Doped Graphene with Pyridinic Dominance as a Highly Active and Stable Electrocatalyst for Oxygen Reduction. *ACS Appl. Mater. Interfaces* **2015**, *7*, 14763−14769.

(25) Chung, H. T.; Won, J. H.; Zelenay, P. Active and Stable Carbon Nanotube/Nanoparticle Composite Electrocatalyst for Oxygen Reduction. *Nat. Commun.* **2013**, *4*, No. 1922.

(26) Wu, Z. S.; Yang, S.; Sun, Y.; Parvez, K.; Feng, X.; Müllen, K. 3D Nitrogen-Doped Graphene Aerogel-Supported Fe_3O_4 Nanoparticles as Efficient Electrocatalysts for the Oxygen Reduction Reaction. *J. Am. Chem. Soc.* **2012**, *134*, 9082−9085.

(27) Lin, Z.; Song, M.; Ding, Y.; Liu, Y.; Liu, M.; Wong, C. Facile Preparation of Nitrogen-Doped Graphene as a Metal-Free Catalyst for Oxygen Reduction Reaction. *Phys. Chem. Chem. Phys.* **2012**, *14*, 3381−3387.

(28) Chung, H. T.; Cullen, D. A.; Higgins, D.; Sneed, B. T.; Holby, E. F.; More, K. L.; Zelenay, P. Direct Atomic-Level Insight into the Active Sites of a High-Performance PGM-Free ORR Catalyst. *Science* **2017**, *357*, 479−484.

(29) Lee, J. S.; Park, G. S.; Kim, S. T.; Liu, M.; Cho, J. A Highly Efficient Electrocatalyst for the Oxygen Reduction Reaction: N-

Doped Ketjenblack Incorporated into Fe/Fe₃C-Functionalized Melamine Foam. *Angew. Chem., Int. Ed.* **2013**, *52*, 1026−1030.

(30) Nishihara, H.; Kyotani, T. Templated Nanocarbons for Energy Storage. *Adv. Mater.* **2012**, *24*, 4473−4498.

(31) Paraknowitsch, J. P.; Zhang, J.; Su, D.; Thomas, A.; Antonietti, M. Ionic Liquids as Precursors for Nitrogen-Doped Graphitic Carbon. *Adv. Mater.* **2010**, *22*, 87−92.

(32) Lee, K. T.; Ji, X.; Rault, M.; Nazar, L. F. Simple Synthesis of Graphitic Ordered Mesoporous Carbon Materials by a Solid-State Method Using Metal Phthalocyanines. *Angew. Chem., Int. Ed.* **2009**, *48*, 5661−5665.

(33) Tang, Y.; Allen, B. L.; Kauffman, D. R.; Star, A. Electrocatalytic Activity of Nitrogen-Doped Carbon Nanotube Cups. *J. Am. Chem. Soc.* **2009**, *131*, 13200−13201.

(34) Sheng, Z. H.; Shao, L.; Chen, J.; Bao, W.; Wang, F.; Xia, X. Catalyst-Free Synthesis of Nitrogen-Doped Graphene via Thermal Annealing Graphite Oxide with Melamine and Its Excellent Electrocatalysis. *ACS Nano* **2011**, *5*, 4350−4358.

(35) Joo, S. H.; Choi, S. J.; Oh, I.; Kwak, J.; Liu, Z.; Terasaki, O.; Ryoo, R. Ordered Nanoporous Arrays of Carbon Supporting High Dispersions of Platinum Nanoparticles. *Nature* **2001**, *412*, 169−172.

(36) Gu, D.; Li, W.; Wang, F.; Bongard, H.; Spliethoff, B.; Schmidt, W.; Weidenthaler, C.; Xia, Y.; Zhao, D.; Schüth, F. Controllable Synthesis of Mesoporous Peapod-like Co₃O₄@Carbon Nanotube Arrays for High-Performance Lithium-Ion Batteries. *Angew. Chem., Int. Ed.* **2015**, *54*, 7060−7064.

(37) Zhang, S.; Miran, M. S.; Ikoma, A.; Dokko, K.; Watanabe, M. Protic Ionic Liquids and Salts as Versatile Carbon Precursors. *J. Am. Chem. Soc.* **2014**, *136*, 1690−1693.

(38) Zhao, D.; Huo, Q.; Feng, J.; Chmelka, B. F.; Stucky, G. D. Nonionic Triblock and Star Diblock Copolymer and Oligomeric Surfactant Syntheses of Highly Ordered, Hydrothermally Stable, Mesoporous Silica Structures. *J. Am. Chem. Soc.* **1998**, *120*, 6024−6036.

(39) Jang, J.; Oh, J. H.; Stucky, G. D. Fabrication of Ultrafine Conducting Polymer and Graphite Nanoparticles. *Angew. Chem., Int. Ed.* **2002**, *41*, 4016−4019.

(40) Ryoo, R.; Joo, S. H.; Jun, S. Synthesis of Highly Ordered Carbon Molecular Sieves via Template-Mediated Structural Transformation. *J. Phys. Chem. B* **1999**, *103*, 7743−7746.

(41) Brunauer, S.; Emmett, P. H.; Teller, E. Adsorption of Gases in Multimolecular Layers. *J. Am. Chem. Soc.* **1938**, *60*, 309−319.

(42) Barrett, E. P.; Joyner, L. G.; Halenda, P. P. The Determination of Pore Volume and Area Distributions in Porous Substances. I. Computations from Nitrogen Isotherms. *J. Am. Chem. Soc.* **1951**, *73*, 373−380.

(43) Bagreev, A.; Menendez, J. A.; Dukhno, I.; Tarasenko, Y.; Bandosz, T. J. Bituminous Coal-Based Activated Carbons Modified with Nitrogen as Adsorbents of Hydrogen Sulfide. *Carbon* **2004**, *42*, 469−476.

(44) Paulus, U. A.; Schmidt, T. J.; Gasteiger, H. A.; Behm, R. J. Oxygen Reduction on a High-Surface Area Pt/Vulcan Carbon Catalyst: A Thin-Film Rotating Ring-Disk Electrode Study. *J. Electroanal. Chem.* **2001**, *495*, 134−145.

(45) Keely, W. M.; Maynor, H. W. Thermal Studies of Nickel, Cobalt, Iron and Copper Oxides and Nitrates. *J. Chem. Eng. Data* **1963**, *8*, 297−300.

(46) Manley, T. R.; Higgs, D. A. Thermal Stability of Melamine Formaldehyde Resins. *J. Polym. Sci., Polym. Symp.* **1973**, *42*, 1377−1382.

(47) Liu, J.; Sun, X.; Song, P.; Zhang, Y.; Xing, W.; Xu, W. High-Performance Oxygen Reduction Electrocatalysts Based on Cheap Carbon Black, Nitrogen, and Trace Iron. *Adv. Mater.* **2013**, *25*, 6879−6883.

(48) Sing, K. S. W.; Everett, D. H.; Haul, R. A. W.; Moscou, L.; Pierotti, R. A.; Rouquérol, J.; Siemieniewska, T. Reporting Physisorption Data for Gas/Solid Systems with Special Reference to the Determination of Surface Area and Porosity. *Pure Appl. Chem.* **1985**, *57*, 603−619.

(49) Jun, S.; Joo, S. H.; Ryoo, R.; Kruk, M.; Jaroniec, M.; Liu, Z.; Ohsuna, T.; Terasaki, O. Synthesis of New, Nanoporous Carbon with Hexagonally Ordered Mesostructure. *J. Am. Chem. Soc.* **2000**, *122*, 10712−10713.

(50) Zhu, J.; Xu, Y.; Zhang, Y.; Feng, T.; Wang, J.; Mao, S.; Xiong, L. Porous and High Electronic Conductivity Nitrogen-Doped Nano-Sheet Carbon Derived from Polypyrrole for High-Power Super-capacitors. *Carbon* **2016**, *107*, 638−645.

(51) Gao, W.; Wan, Y.; Dou, Y.; Zhao, D. Synthesis of Partially Graphitic Ordered Mesoporous Carbons with High Surface Areas. *Adv. Energy Mater.* **2011**, *1*, 115−123.

(52) Chen, W.; Pan, X.; Bao, X. Tuning of Redox Properties of Iron and Iron Oxides via Encapsulation within Carbon Nanotubes. *J. Am. Chem. Soc.* **2007**, *129*, 7421−7426.

(53) Tuinstra, F.; Koenig, L. Raman Spectrum of Graphite. *J. Chem. Phys.* **1970**, *53*, 1126−1130.

(54) Ramm, M.; Ata, M.; Brzezinka, K.; Gross, T.; Unger, W. Studies of Amorphous Carbon Using X-Ray Photoelectron Spectroscopy, near-Edge X-Ray-Absorption Fine Structure and Raman Spectroscopy. *Thin Solid Films* **1999**, *354*, 106−110.

(55) Dippel, B.; Jander, H.; Heintzenberg, J. NIR FT Raman Spectroscopic Study of Flame Soot. *Phys. Chem. Chem. Phys.* **1999**, *1*, 4707−4712.

(56) Sadezky, A.; Muckenhuber, H.; Grothe, H.; Niessner, R.; Pöschl, U. Raman Microspectroscopy of Soot and Related Carbonaceous Materials: Spectral Analysis and Structural Information. *Carbon* **2005**, *43*, 1731−1742.

(57) Lee, J.; Yoon, S.; Hyeon, T.; Oh, S. M.; Kim, K. B. Synthesis of a New Mesoporous Carbon and Its Application to Electrochemical Double-Layer Capacitors. *Chem. Commun.* **1999**, 2177−2178.

(58) Wei, D.; Liu, Y.; Wang, Y.; Zhang, H.; Huang, L.; Yu, G. Synthesis of N-Doped Graphene by Chemical Vapor Deposition and Its Electrical Properties. *Nano Lett.* **2009**, *9*, 1752−1758.

(59) Ferrandon, M.; Kropf, A. J.; Myers, D. J.; Artyushkova, K.; Kramm, U.; Bogdano, P.; Wu, G.; Johnston, C. M.; Zelenay, P. Multitechnique Characterization of a Polyaniline-Iron-Carbon Oxygen Reduction Catalyst. *J. Phys. Chem. C* **2012**, *116*, 16001−16013.

(60) Othman, R.; Dicks, A. L.; Zhu, Z. Non Precious Metal Catalysts for the PEM Fuel Cell Cathode. *Int. J. Hydrogen Energy* **2012**, *37*, 357−372.

(61) Li, Y.; Zhou, W.; Wang, H.; Xie, L.; Liang, Y.; Wei, F.; Idrobo, J.-C.; Pennycook, S. J.; Dai, H. An Oxygen Reduction Electrocatalyst Based on Carbon Nanotube-graphene Complexes. *Nat. Nanotechnol.* **2012**, *7*, 394−400.

(62) Faubert, G.; Côté, R.; Dodelet, J.-P.; Lefèvre, M.; Bertrand, P. Oxygen Reduction Catalysts for Polymer Electrolyte Fuel Cells from the Pyrolysis of Fe^II Acetate Adsorbed on 3,4,9,10-Perylenetetracarboxylic Dianhydride. *Electrochim. Acta* **1999**, *44*, 2589−2603.

(63) Ikeda, T.; Boero, M.; Huang, S. F.; Terakura, K.; Oshima, M.; Ozaki, J. Carbon Alloy Catalysts: Active Sites for Oxygen Reduction Reaction. *J. Phys. Chem. C* **2008**, *112*, 14706−14709.

(64) Yang, W.; Liu, X.; Yue, X.; Jia, J.; Guo, S. Bamboo-like Carbon nanotube/Fe₃C Nanoparticle Hybrids and Their Highly Efficient Catalysis for Oxygen Reduction. *J. Am. Chem. Soc.* **2015**, *137*, 1436−1439.

(65) Buan, M. E. M.; Muthuswamy, N.; Walmsley, J. C.; Chen, D.; Rønning, M. Nitrogen-Doped Carbon Nanofibers on Expanded Graphite as Oxygen Reduction Electrocatalysts. *Carbon* **2016**, *101*, 191−202.

(66) Yang, D.-S.; Song, M. Y.; Singh, K. P.; Yu, J.-S. The Role of Iron in the Preparation and Oxygen Reduction Reaction Activity of Nitrogen-Doped Carbon. *Chem. Commun.* **2015**, *51*, 2450−2453.

(67) Qian, Y.; Du, P.; Wu, P.; Cai, C.; Gervasio, D. F. Chemical Nature of Catalytic Active Sites for the Oxygen Reduction Reaction on Nitrogen-Doped Carbon-Supported Non-Noble Metal Catalysts. *J. Phys. Chem. C* **2016**, *120*, 9884−9896.

(68) Osmieri, L.; Monteverde Videla, A. H. A.; Armandi, M.; Specchia, S. Influence of Different Transition Metals on the Properties of Me-N-C (Me = Fe, Co, Cu, Zn) Catalysts Synthesized

Using SBA-15 as Tubular Nano-Silica Reactor for Oxygen Reduction Reaction. *Int. J. Hydrogen Energy* **2016**, *41*, 22570−22588.

(69) Banham, D.; Ye, S.; Pei, K.; Ozaki, J.-I.; Kishimoto, T.; Imashiro, Y. A Review of the Stability and Durability of Non-Precious Metal Catalysts for the Oxygen Reduction Reaction in Proton Exchange Membrane Fuel Cells. *J. Power Sources* **2015**, *285*, 334−348.

(70) Chu, Y. H.; Shul, Y. G. Alcohol Crossover Behavior in Direct Alcohol Fuel Cells (DAFCs) System. *Fuel Cells* **2012**, *12*, 109−115.